SCIENTIFIC REPORTS

OPEN

SUBJECT AREAS:
SYNTHESIS AND PROCESSING
POROUS MATERIALS
SURFACES, INTERFACES AND THIN FILMS
NANOPARTICLES

Received
18 June 2013

Accepted
27 August 2013

Published
25 September 2013

Correspondence and requests for materials should be addressed to X.D.X. (xiaoxd@ms.giec.ac.cn) or G.X. (xugang@ms.giec.ac.cn)

Anisotropic vanadium dioxide sculptured thin films with superior thermochromic properties

Yaoming Sun[1], Xiudi Xiao[1], Gang Xu[1], Guoping Dong[2], Guanqi Chai[1], Hua Zhang[1], Pengyi Liu[3], Hanmin Zhu[3] & Yongjun Zhan[1]

[1]Key Laboratory of Renewable Energy and Gas Hydrates, Guangzhou Institute of Energy Conversion, Chinese Academy of Sciences, Guangzhou, 510640 P. R. China, [2]State Key Laboratory of Luminescent Materials and Devices,South China University of Technology, Guangzhou, 510640 P. R. China, [3]Jinan University, Guangzhou, 510640 P. R. China.

VO_2 (M) STF through reduction of V_2O_5 STF was prepared. The results illustrate that V_2O_5 STF can be successfully obtained by oblique angle thermal evaporation technique. After annealing at 550°C/3 min, the V_2O_5 STF deposited at 85° can be easily transformed into VO_2 STF with slanted columnar structure and superior thermochromic properties. After deposition SiO_2 antireflective layer, T_{lum} of VO_2 STF is enhanced 26% and ΔT_{sol} increases 60% compared with that of normal VO_2 thin films. Due to the anisotropic microstructure of VO_2 STF, angular selectivity transmission of VO_2 STF is observed and the solar modulation ability is further improved from 7.2% to 8.7% when light is along columnar direction. Moreover, the phase transition temperature of VO_2 STF can be depressed into 54.5°C without doping. Considering the oblique incidence of sunlight on windows, VO_2 STF is more beneficial for practical application as smart windows compared with normal homogenous VO_2 thin films.

Monoclinic/rutile (M/R)-phase VO_2, due to its reversible metal-insulator (MIT) phase transitions, has attracted great attention in many fields, such as resistive switching elements[1], smart windows[2], light modulators[3] and optical storage devices[4], etc. With the energy supply tension and the rise of energy-saving technology, VO_2-based smart window becomes the focus due to its optical modulation ability in infrared spectra region. However, a low luminous transmittance (T_{lum}) and solar modulating ability (ΔT_{sol}) are the two major drawbacks for the practical application of VO_2-base smart windows[5]. The T_{lum} and T_{sol} values were obtained from $T_{lum,sol}(\tau) = \int \varphi_{lum,sol}(\lambda)T(\lambda,\tau)d\lambda / \int \varphi_{lum,sol}(\lambda)d\lambda$, where φ_{lum} is the spectral sensitivity of the light-adapted eye and φ_{sol} is the solar irradiance spectrum for an air mass 1.5 (corresponding to the sun standing 37° above the horizon). ΔT_{sol} is obtained from $\Delta T_{sol} = T_{sol,l} - T_{sol,h}$, where l and h denote low- and high-temperature, respectively.

Different strategies are investigated to improve T_{lum} and ΔT_{sol}, including Mg- or F-doping[6,7], multilayer-stack design[8,9], composite film construction[10,11], nanoporous incorporation[12]. Mg- or F-doping causes both the depression of transition temperature and a blue shift in the absorption edge of VO_2 films (from around 445 to 415 nm[6]). A blue shift of absorption edge results in a significant increase of luminous transmittance with the expense of infrared modulating ability[7]. The competitive relation between luminous transmittance and solar modulation ability has also been observed in VO_2 based multilayer films[8]. A VO_2-SiO_2 composite films show a high luminous transmittance but weak infrared modulating ability[10]. Optical calculations suggest that VO_2 nanoparticles distributed in a transparent dielectric matrix can show higher T_{lum} and ΔT_{sol}[13]. Gao et al.[11] have proved that VO_2-based composite thin films show superior luminous transmittance and solar modulation ability. However, compared with other dielectric matrix, porosity shows much more advantages, such as low refractive index, good compatibility and flexible adjustability. Kang et al.[12] have proved that nanoporous VO_2 thin films prepared by spinning method can enhance the luminous transmittance and solar modulation ability. However, investigation on nanoporous VO_2 thin films prepared by physical vapor deposition is seldom.

Oblique angle deposition (OAD) technique is a common technique to adjust the porosity and microstructure of thin films, which is named sculptured thin films (STF)[14]. Sculptured thin films with controllable porosity and microstructure can show gradual optical constants and special physical properties, which can be used in many fields, such as rugate filters[15], sensors[16], phase retarder[17], etc. The adjustable optical constants of STF are beneficial for the optical design of multilayer thin films and the dielectric layer is more optional. The anisotropic

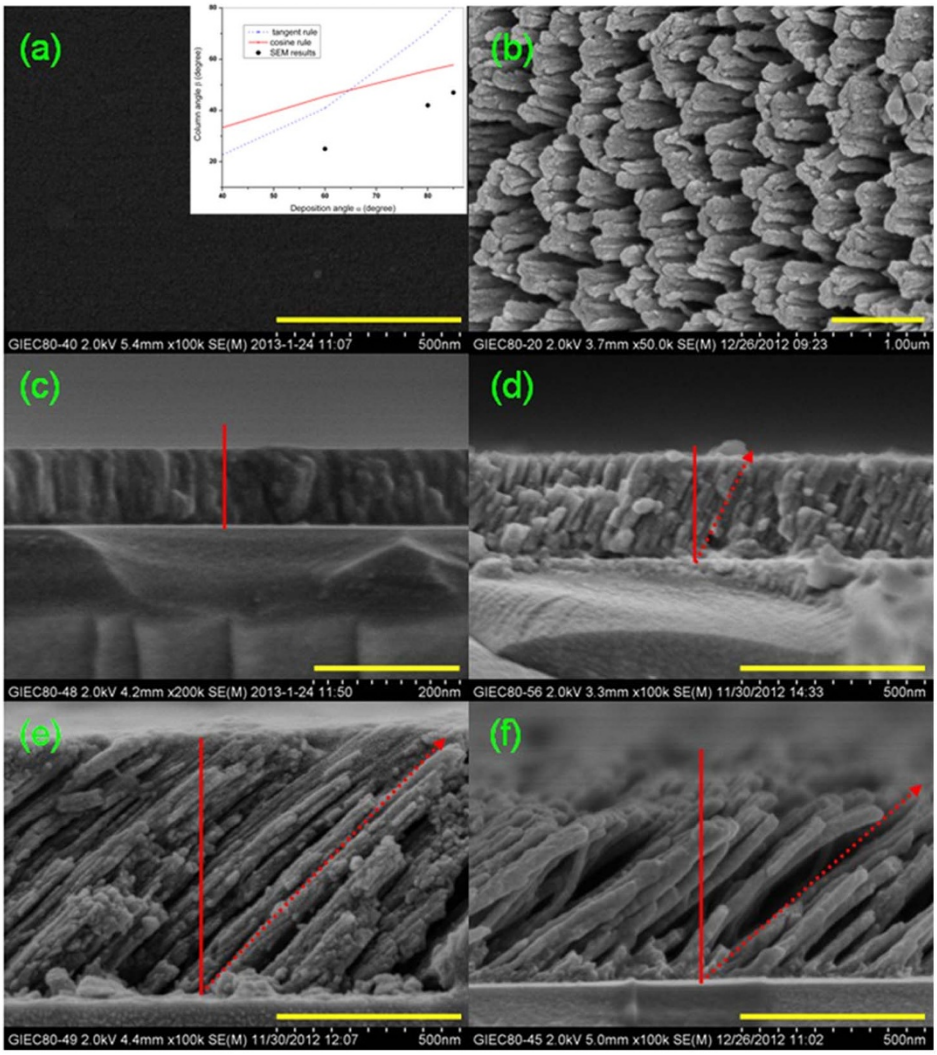

Figure 1 | **SEM surface and cross-sectional images of as-deposited V_2O_5 sculptured thin films deposited at different oblique angle.** (a, c) 0°; (b, f) 85°; (d) 60°; (e) 80°. The scale bar in Fig. 1 (c) is 200 nm. The other scale bar is 500 nm.

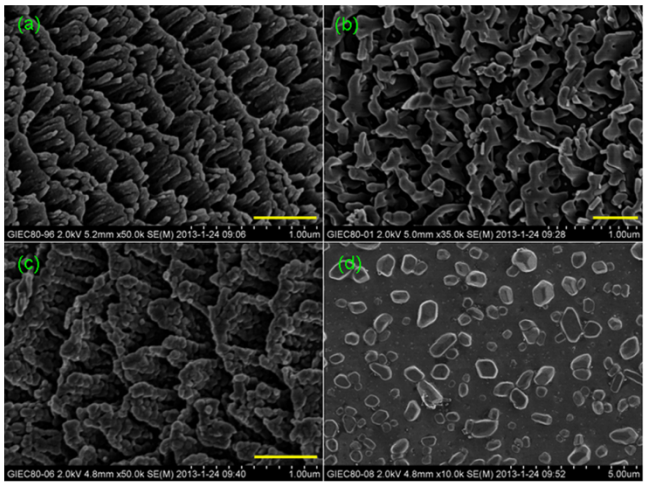

Figure 2 | **SEM images of V_2O_5 sculptured thin films deposited at 85° after annealing at different temperature for 5 min.** (a) 500°C; (b) 550°C; (c) 600°C; (d) 700°C. The scale bar is 500 nm.

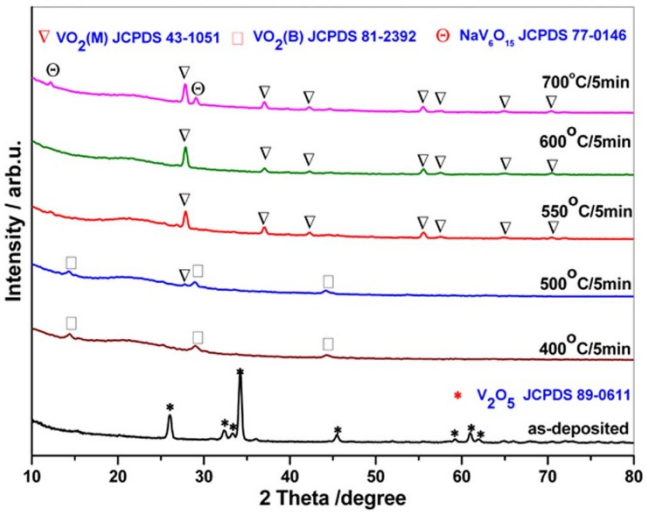

Figure 3 | **XRD patterns of V_2O_5 sculptured thin films deposited at 85° after annealing at different temperature for 5 min.**

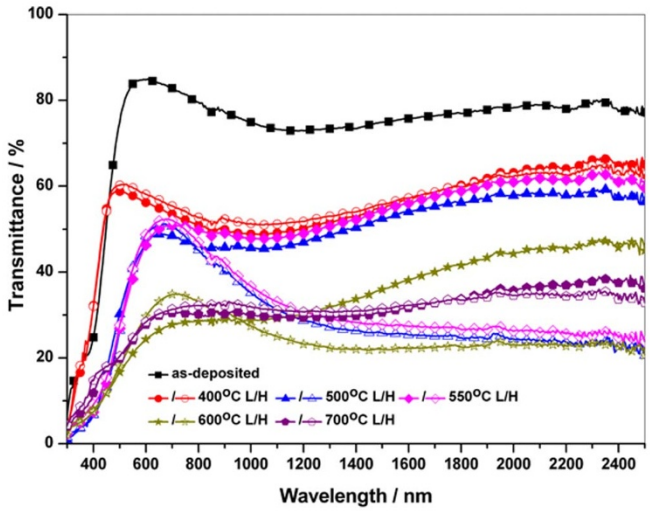

Figure 4 | Transmittance spectra of V_2O_5 sculptured thin films deposited at 85° after annealing at different temperature for 5 min.

microstructure of STF can show angular selectivity transmission. Combination with VO_2 thin films and OAD technique, it is supposed that VO_2 STF can show superior luminous transmittance and solar modulation ability. In present paper, the optical properties and phase transition process of VO_2 STF were investigated. The results illustrated that VO_2 STF with slanted columnar structure can show superior thermochromic properties and angular selectivity transmission, which can be improved by antireflective layer design. The phase transition temperature of VO_2 STF can be depressed into 54.5°C without doping, which is superior to normal VO_2 film without doping. Due to the porosity, the refractive index of antireflective layer can be smaller than 2. Combination of SiO_2 antireflective layer and angular selectivity transmittance, ΔT_{sol} can be enhanced from 4.5% to 8.7%. Considering the oblique incidence of sunlight on windows, VO_2 STF is supposed as the most suitable candidate as smart windows.

Results

V_2O_5 sculptured thin films. SEM images of as-deposited V_2O_5 STF deposited at different angles are shown in **Fig. 1**. It can be found that the thin films are porous with OAD technique (see **Fig. 1(a, b)**). With the increase of deposition angle, films are with slanted columnar structure. The columns incline towards the direction of the incoming flux. The higher the deposition angle is, the greater the column inclination is. The highly orientated nanostructure of the slanted columns indicates that V_2O_5 films are anisotropy[19], with the long axis parallel to the columnar growth direction. The anisotropic structure will introduce the anisotropic dependence into the thermal, electrical, magnetic and optical properties of thin films[20].

Column angle β, defined as the angle between substrate surface normal and the long axis of slanted columns, is a significant structural parameter. As can be seen, the column angle increases with the increase of deposition angle. There are two empirical formulae developed to estimate column angle at oblique incidence: (1) tangent rule ($\tan\beta = 0.5\tan\alpha$, $\alpha < 70^\circ$)[21]; (2) cosine rule ($2\sin(\alpha-\beta) = 1-\cos\alpha$, $\alpha > 70^\circ$)[22]. However, the experimental column angle measured from SEM images is about 25°, 42°, 47° for α = 60, 80, 85°, respectively, which are rather lower than the value estimated by the tangent rule ($\beta = 40.9^\circ$ at $\alpha = 60$) and cosine rule ($\beta = 55.6^\circ$ at $\alpha = 80^\circ$ and $\beta = 57.8^\circ$ at $\alpha = 85^\circ$). The origin of the deviation may be due to the great surface curvature of nanostructure films grown by OAD. This will distinctly change the direction of column angle compared to that of micro-sized thin films. Additionally, the column angle also depends on the deposited material. Hodgkinson and Wu proposed the modified tangent rule ($\tan\beta = E_1\tan\alpha$) and the parameter E_1 is variable with different materials[23]. As to V_2O_5 STF, the relationship between β and α obeys exponential function fitted by the results of SEM measurements (see the insert of **Fig. 1 (a)**).

The effect of annealing temperature. It is well-known that deposition angle is an important factor to sculpture films structure by OAD technique. However, in our experiment, VO_2 (M) STF is indirectly obtained through V_2O_5 STF. It can be deduced that annealing conditions can play a great effect on the microstructure of VO_2 (M).

To obtain VO_2 STF, V_2O_5 STF was reduced in hydrogen atmosphere. After annealing, the morphology and structure of STF were greatly changed just as shown in **Fig. 2**. According to the SEM images of V_2O_5 STF annealed at different temperature, it can be found that the columnar structure become aggregation. The gap between columns in the same row is decreasing after annealing at 500°C. When the annealing temperature is up to 550°C, the intact columnar structure can not be observed and conglutination appears between columns. When the annealing temperature reaches 600°C, distinct particles on columns are observed and the single column becomes thick. When annealing temperature is up to 700°C, no column and porosity is observed and only polygonal particles disperse on the film surface. It means the sculptured thin films are completely destroyed at 700°C.

The XRD patterns of V_2O_5 STF annealed at different temperature are shown in **Fig. 3**. It can be found that as-deposited thin film is polycrystalline with apparent peaks in XRD pattern, which is different from other oxide STF by evaporation method[18]. The peaks are ascribed to V_2O_5 (JCPDS 89-0611). After annealing at hydrogen atmosphere, peaks ascribed to V_2O_5 disappear and some peaks ascribed to VO_2 (B) (JCPDS 81-2392) are observed. With the increase of annealing temperature, the peaks of VO_2 (B) are firstly enhanced at 500°C and then disappear at 550°C. When annealing temperature is higher than 550°C, no peaks of VO_2 (B) is observed and peaks ascribed to VO_2 (M) (JCPDS 43-1051) appear. It is known that VO_2 (B) can be transformed into VO_2 (M) at high temperature[24]. However, the transformation temperature is higher than that observed in VO_2 (B) powder at inert atmosphere[25]. According to our previous results on VO_2 (B) prepared by hydrothermal method, lower crystallinity of VO_2 (B) needs low transformation temperature[25]. In present paper, the higher transformation temperature of VO_2 (B) may be resulted from the different structure of thin film and

Table I | T_{lum}, ΔT_{lum}, T_{sol}, ΔT_{sol}, T_{2000}, ΔT_{2000} of V_2O_5 STF deposited at 85° after annealing at different temperature

	T_{lum}[%]			T_{sol}[%]			T_{2000}[%]		
	30°C	100°C	ΔT_{lum}	30°C	100°C	ΔT_{sol}	30°C	100°C	ΔT_{2000}
400°C	57.3	59.1	−1.8	52	53.4	−1.4	63.1	62.3	0.8
500°C	40.7	40.9	−0.2	40.6	34.3	6.3	57.8	24.4	33.3
550°C	39	41.1	−2.1	41.5	35.7	5.8	61.0	26.2	34.8
600°C	21.4	25.1	−3.7	25	24.8	0.2	44.3	23.2	21.1
700°C	24.7	25.2	−0.5	26.5	27.6	−1.1	35.7	34.5	1.2

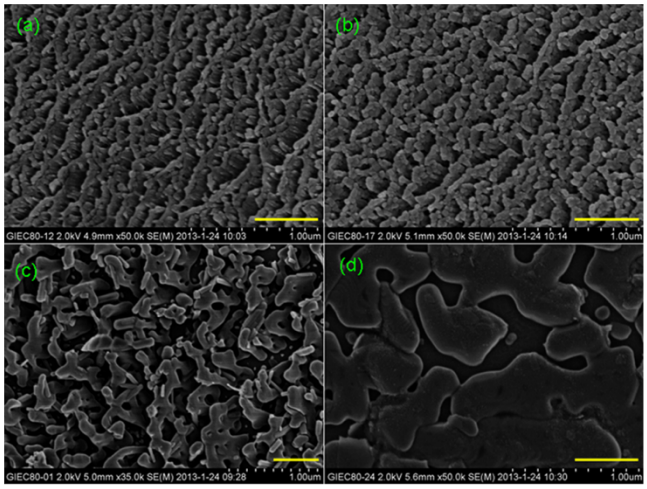

Figure 5 | SEM images of V_2O_5 sculptured thin films deposited at 85° after annealing at 550°C for different time. (a) 1 min; (b) 3 min; (c) 5 min; (d) 8 min. The scale bar is 500 nm.

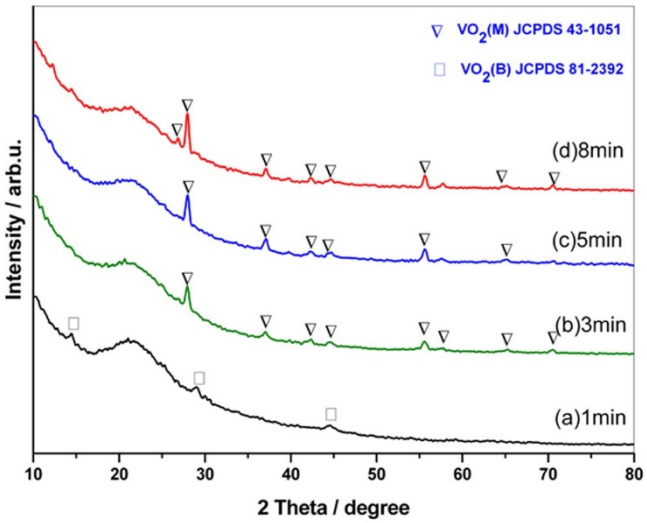

Figure 6 | XRD patterns of V_2O_5 sculptured thin films deposited at 85° after annealing at 550°C for different time. (a) 1 min; (b) 3 min; (c) 5 min; (d) 8 min.

preparation process. With the increase of annealing temperature, the peaks ascribed to VO_2 (M) are enhanced. When V_2O_5 STF is annealed at 700°C, two peaks at 12.2° and 29.2° appear, which can be ascribed to NaV_6O_{15} (JCPDS 77-0146). It is inferred that sodium is from the glass substrate and high temperature is beneficial for the diffusion of Na^+ ions, which finally result in the formation of NaV_6O_{15}.

Transmission spectra of V_2O_5 STF after annealing are shown in **Fig. 4**. It can be found that as-deposited V_2O_5 STF show high transmission. After annealing, the transmission is reduced and the UV cut-off edge shifts to longer wavelength, which is resulted from the transformation of V_2O_5 to VO_2. According to the high (H) and low (L) temperature transmission spectra of VO_2 STF, the MIT transition is clearly observed as a dramatic infrared-transmittance change with temperature. The change of transmittance value is compiled in **Table I**.

It can be found that STF annealing at 400°C shows high T_{lum} and weak ΔT_{sol}. With the increase of annealing temperature, the T_{lum} is gradually decreasing while the ΔT_{sol} is firstly increasing and then decreasing. It is known that the VO_2 (B) with broad band gap can show relatively high visible transmittance and T_{lum}, while it cannot produce reversible phase transition below 100°C. Thus, V_2O_5 STF annealing at 400°C mainly containing VO_2 (B) does not show apparent infrared-transmission change (see Fig. 2). The decreasing of T_{lum} and increasing of ΔT_{sol} is resulted from the increasing content of VO_2 (M). Theoretically, the improved crystallinity and content of VO_2 (M) can result in the increase of ΔT_{sol}. However, the ΔT_{sol} is decreasing for V_2O_5 STF annealing at 600°C and 700°C. For V_2O_5 STF annealing at 600°C, the aggregation of columns augment the distance of columns and minify the columnar angle, which result in the decreasing of columnar density and effective content of VO_2(M) in fixed light spot size of transmittance testing. Thus, the ΔT_{sol} is still decreasing for thin films with superior crystallinity. For STF annealed at 700°C, VO_2 (M) particles are much more dispersive and the existence of NaV_6O_{15} reduces the content of VO_2 (M). Therefore, STF annealed at 700°C show weak ΔT_{sol}. Conventionally, the transmittance change at wavelength of 2000nm is another factor to evaluate the spectral modulation ability. According to the transmittance spectra, ΔT_{2000} is also shown in **Table I**. The change of ΔT_{2000} is consistent with the change of ΔT_{sol}, which is further proved our above mentioned analysis. According to the optical properties and microstructure of thin films, it can be deduced that the optimum annealing temperature is about 550°C.

The effect of annealing time. SEM images of V_2O_5 STF after annealing at 550°C for different time are shown in **Fig. 5**. It can be found that short time heat treatment does no effect on the morphology of thin films, which are still porous with slanted columns. With the elongation of annealing time, the particles grow up and some columns begin aggregation. When annealing time is up to 5 min, some columns begin to melt and become coarse. The pores between columns are enlarging. When annealing time reaches 8 min, no columns can be observed. Only abnormal bulk-like structures with big pores are existent on the film surface, which means that the regular porous columnar structure is completely destroyed after long time heat treatment.

The XRD patterns of V_2O_5 STF annealing at 550°C for different time are shown in **Fig. 6**. It can be found that only several weak peaks appear in the XRD pattern of V_2O_5 STF annealing for 1 min, which are ascribed to VO_2 (B). When the annealing time reaches 3 min, thin films completely transform into VO_2 (M).

The transmission spectra of V_2O_5 STF annealing at 550°C for different time are shown in **Fig. 7**. It can be found that the transmission is decreasing with the increase of annealing time and the UV

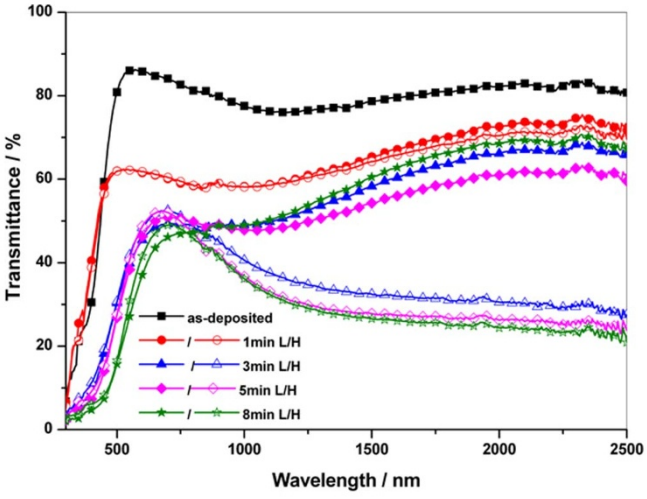

Figure 7 | Transmittance spectra of V_2O_5 sculptured thin films deposited at 85° after annealing at 550°C for different time.

Table II | T_{lum}, ΔT_{lum}, T_{sol}, ΔT_{sol}, T_{2000}, ΔT_{2000} of V_2O_5 STF deposited at 85° after annealing at 550°C for different time

	T_{lum} [%]			T_{sol}[%]			T_{2000}[%]		
	30°C	100°C	ΔT_{lum}	30°C	100°C	ΔT_{sol}	30°C	100°C	ΔT_{2000}
1 min	61.8	61.9	−0.1	59	58.6	0.4	72.6	70.4	2.2
3 min	40	42.1	−2.1	42.8	38.2	4.6	66.2	30.6	35.6
5 min	39	41.1	−2.1	41.5	35.7	5.8	61.0	26.2	34.8
8 min	28.7	32.1	−3.4	38.4	31.9	6.5	68.5	24.4	44.1

cut-off edge shifts to longer wavelength, which means that the content of VO_2 (M) is increasing with annealing time. According to transmission spectra, the T_{lum} and ΔT_{sol} are compiled in **Table II**. The T_{lum} is decreasing with the increasing annealing time and ΔT_{sol} is increasing with annealing time, which is consistent with the result in XRD patterns (**see Fig. 6**). It means that long annealing time is beneficial for high crystallinity of VO_2 (M) and superior solar modulation ability. However, the columnar structure can be destroyed when annealing time is longer than 5 min. Therefore, in the following works, we choose a moderate annealing time of 3 min to investigate the microstructure and optical properties of thin films.

The effect of deposition angle. The morphology of V_2O_5 STF deposited at different oblique angles after annealing at 550°C/3 min are shown in **Fig. 8**. It can be found that the morphology was greatly changed after annealing. For V_2O_5 thin films deposited at 0°, the film is compact (see **Fig. 1**). After annealing, the films become porous with abnormal structure on the surface. While for V_2O_5 thin films deposited at 60°, the columnar structure is completely destroyed after annealing and only some belt like particles are existent on the surface. For V_2O_5 thin films deposited at 80°, the surface is like melted after annealing and the columns aggregates which make the column more inclined with higher column angle. The column angle is about 60°, but the arrangement of columns is not regular compared with as-deposited V_2O_5 STF at 80°. For V_2O_5 thin films deposited at 85°, the morphology and column structure is almost constant after annealing except for the increased column angle. It is known that large column angle can result in large anisotropy and high porosity, which can resulted in low refractive index and high visible transmission.

Transmittance spectra of V_2O_5 STF deposited at different oblique angles after annealing at 550°C/3 min are shown in **Fig. 9**. It can be found that the transmittance is remarkably enhancing with the increase of deposition angle. It is proposed that the increase of deposition angle can increase the porosity in films and reduce the refractive index of films, which can result in the increase of transmission[18]. For film deposited at 85°, the ultraviolet cut-off edge of VO_2 (M) STF is even smaller than 400 nm, which means that optical band gap is increased and the refractive index is sharply reduced by deposition angle adjustment[18]. The optical properties of T_{lum} and ΔT_{sol} are compiled in Table III.

Discussion

It can be found that T_{lum} is increasing with deposition angle while the variation of ΔT_{sol} is not consistent with T_{lum} in Table III. Generally, the visible transmittance at 30°C is lower than that at 100°C (see Table I and II). However, the visible transmittance at 30°C of 0° deposited film exceeds that at 100°C (see Table III). Xu et al.[26] and Kang et al.[12] proposed that film thickness dependent interference effects can result in the reversion of ΔT_{lum}. In view of the fact that solar energy is mainly in the visible region with a peak at 550 nm, the ΔT_{lum} reversion across the MIT greatly influences ΔT_{sol}. Thus, film deposited at 0° shows larger ΔT_{sol} than that of films deposited at other deposition angle. However, the absolute value of ΔT_{lum} reversion is decreasing with the increase of deposition angle and the ΔT_{sol} rises up after a fall. Factually, the solar modulation ability (ΔT_{sol}) is related with both ΔT_{lum} and infrared modulation (ΔT_{2000}). The variation of ΔT_{2000} is resulted from the crystallinity, content and film structure of VO_2 (M). The increase of deposition angle can result in the high porosity and relative low content of VO_2 (M) as well as low infrared modulation. Thus, films deposited at 85° show high visible transmittance and relative low solar ability.

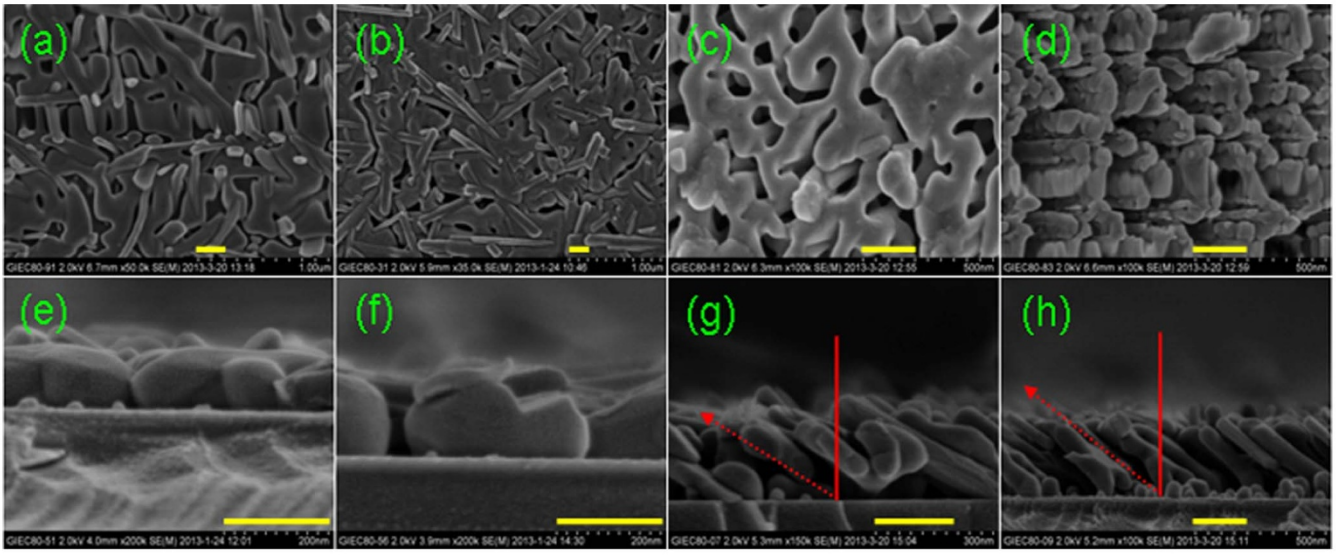

Figure 8 | SEM surface and cross-sectional images of V_2O_5 sculptured thin films deposited at different oblique angles after annealing at 550°C/3 min. (a, e) 0°; (b, f) 60°; (c, g) 80°; (d, f) 85°. The scale bar is 200 nm.

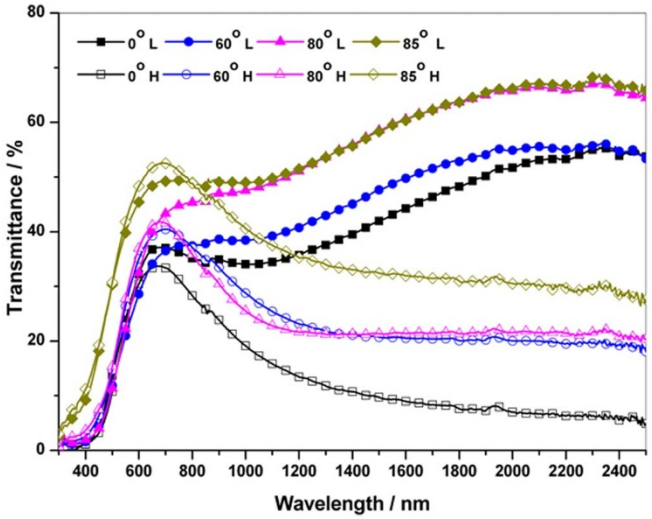

Figure 9 | Transmittance spectra of V_2O_5 sculptured thin films deposited at different oblique angles after annealing at 550°C/3 min.

To determine the phase-transition temperature of the VO_2 STF, hysteresis loops of pure and tungsten-doped VO_2 STF were measured by recording transmittances and temperatures of STF at a fixed optical wavelength (2000 nm). As seen in **Fig. 10**, pure VO_2 film shows hysteresis loop width of 6°C at mean transmittance, which is consistent with that of pure VO_2 film on glass[10]. The mean phase transition temperature (T_t) is about 54.5°C, which is much lower than that of pure VO_2 films (68°C) deposited by other methods[10,27]. It is known that phase transition temperature can be depressed by doping, finite size and inhomogeneous strain[28,29]. For VO_2 STF without doping, films are porous with tilted columnar structure and the residual stress is huge[30]. It can be deduced that the depressed phase transition temperature may be resulted form inhomogeneous strain in film. After tungsten doping, VO_2 films exhibited a hysteresis loop centered at 35.8°C with a width of 9.7°C, implying a decrease in the phase transition temperature of about 17.7°C. This decreasing efficiency is less than that described in other reports[31,32], likely because the tungsten ions were not completely incorporated into the final VO_2 films. The width widening of the hysteresis loop can be attributed to the states of grain boundaries and defects introduced by tungsten doping. It is known that tungsten doping can result in both the decrease of temperature and infrared modulation ability. The VO_2 STF without doping can show superior infrared modulation ability and equal transition temperature compared with VO_2 thin films with doping.

Deposition antireflective layer is an important factor to improve luminous transmittance. Generally, antireflective layer with refractive index about $2 \sim 2.5$ is proposed as the superior material for common VO_2 film[9]. Considering VO_2 STF deposited by OAD technique with gradient refractive index, refractive index of antireflective layer can be lower than 2. Though the real refractive index of VO_2 STF was not tested due to the limit of instrument, silicon dioxide with refractive index about 1.46 ($\lambda = 550$ nm) was used as antireflective layer to prove our supposition. The transmission spectra of V_2O_5 STF deposited at 0° and 85° after annealing at 550°C/3 min before and after SiO_2 antireflective layer deposition are shown in **Fig. 11**. It can be found that the transmission spectra are greatly changed after antireflective layer deposition with the same thickness. For films deposited at 0°, besides the increase of transmission, the position of interference peaks was not changed after SiO_2 layer deposition. While for films deposited at 85°, the position of interference peak shifts to shorter wavelength accompanying with the enhanced transmittance. The reason may be that relatively smaller equivalent thickness and the low refractive index of VO_2 films deposited at 85° show strong interferences with SiO_2 antireflective layer, which results in the blue shift of interferences peaks. The T_{lum} and ΔT_{sol} are compiled in Table IV. After SiO_2 deposition, T_{lum} of VO_2 film deposited at 0° increases 20% (32.7% to 39.5%) and ΔT_{sol} increases 15% (6.6% to 7.6%), while T_{lum} of VO_2 film deposited at 85° is enhanced 26% (36.9% to 46.6%) and ΔT_{sol} increases of 60% (4.5% to 7.2%), which means that SiO_2 antireflective layer is much more effective to improve luminous transmission and solar modulation ability of VO_2 STF than normal VO_2 films.

It is known that VO_2 STF with slanted columnar structure can show anisotropy optical properties. The transmission of STF along and perpendicular to column direction is obviously different. For convenience to prove, transmission spectra of 0° and ±30° incidence are shown in **Fig. 12**. T_{lum} and ΔT_{sol} according to transmission spectra are compiled in **Table V**. For VO_2 deposited at 0°, T_{lum} and ΔT_{sol} of +30° light incidence are almost the same with that of −30° light incidence, but it is much smaller than that of 0° incidence. For the homogeneous film, transmission of light oblique incidence is smaller than that of normal incidence according to interference optics. However, the result is absolutely different for anisotropic VO_2 STF. For VO_2 deposited at 85°, T_{lum} of +30° light incidence is smaller than that of −30° and 0° light incidence, but ΔT_{sol} is higher than that of −30° and 0° incidence. The reason may be that +30° light incidence is along columnar direction and the effective thickness of VO_2 (M) is larger than that of −30° and 0° light incidence. Thus, T_{lum} is relatively smaller than that of −30° and 0° light incidence and ΔT_{sol} is higher than that of −30° and 0° light incidence. For VO_2 deposited at 85° with SiO_2 antireflective layer, ΔT_{sol} of +30° light incidence is enhanced 20% with only 4% decrease of T_{lum} compared with normal incidence. Factually, sunlight is oblique incidence onto windows, the angle selective transmission of VO_2 STF is more beneficial for practical application.

Considering the polarization effect and anisotropy of STF films, the polarization transmittance spectra are shown in **Fig. 13**. For VO_2 films deposited at 0°, films are homogenous. There is no polarization effect observed when polarization light is 0° incidence just as see in **Fig. 13 (a)**. While the transmission spectra of P-light and S-light are divided and polarization effect happens when incidence angel is 30°. For VO_2 deposited at 85°, films are anisotropy with slanted columns. The P and S lights are separated and the transmission spectra cannot be overlapped when polarization incidence is 0° (see **Fig. 13 (d)**), which means the optical anisotropy is observed in VO_2 STF and is consistent with the results in other oxides films[18,23]. When incident light is oblique, the polarization effect is amplified just as see in

Table III | T_{lum}, ΔT_{lum}, T_{sol}, ΔT_{sol}, T_{2000}, ΔT_{2000} of V_2O_5 STF deposited at different angles after annealing at 550°C/3 min

	T_{lum} [%]			T_{sol}[%]			T_{2000}[%]		
Deposition angle(α)	30°C	100°C	ΔT_{lum}	30°C	100°C	ΔT_{sol}	30°C	100°C	ΔT_{2000}
0°	25.1	23.3	1.8	28.9	19	10	51.7	7.0	44.7
60°	22.1	27.3	−5.2	29.6	25.9	3.7	54.9	20.0	34.9
80°	24.1	28.8	−4.7	35.6	25.9	9.7	65.7	21.5	44.2
85°	40	42.1	−2.1	42.8	38.2	4.6	66.2	30.6	35.6

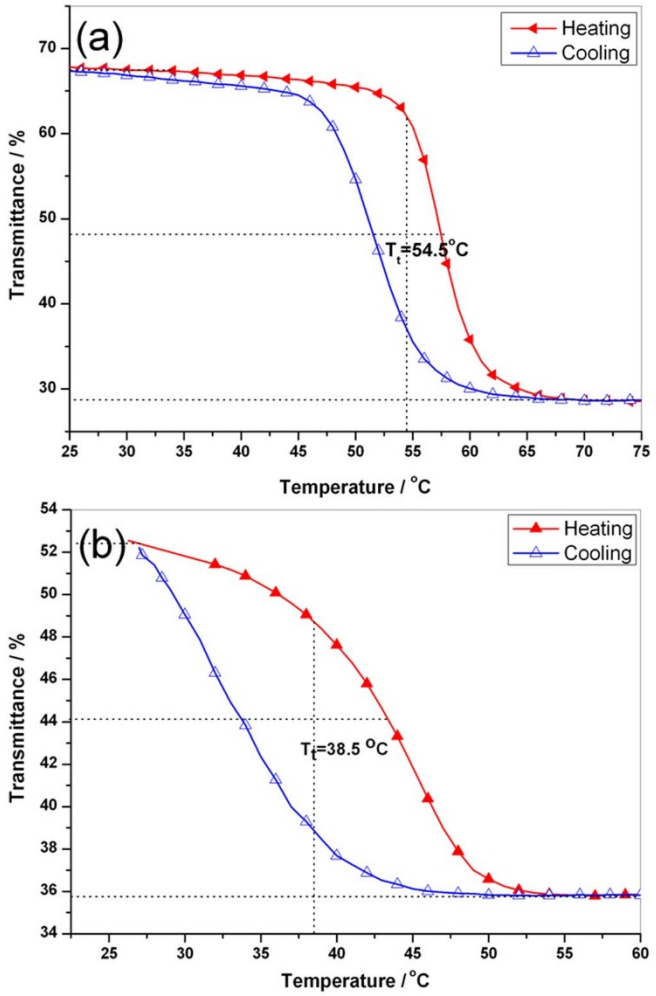

Figure 10 | Thermal hystersis loops of V_2O_5 thin films deposited at 85° after annealing at 550°C/3 min. (a) without doping; (b) with tungsten doping.

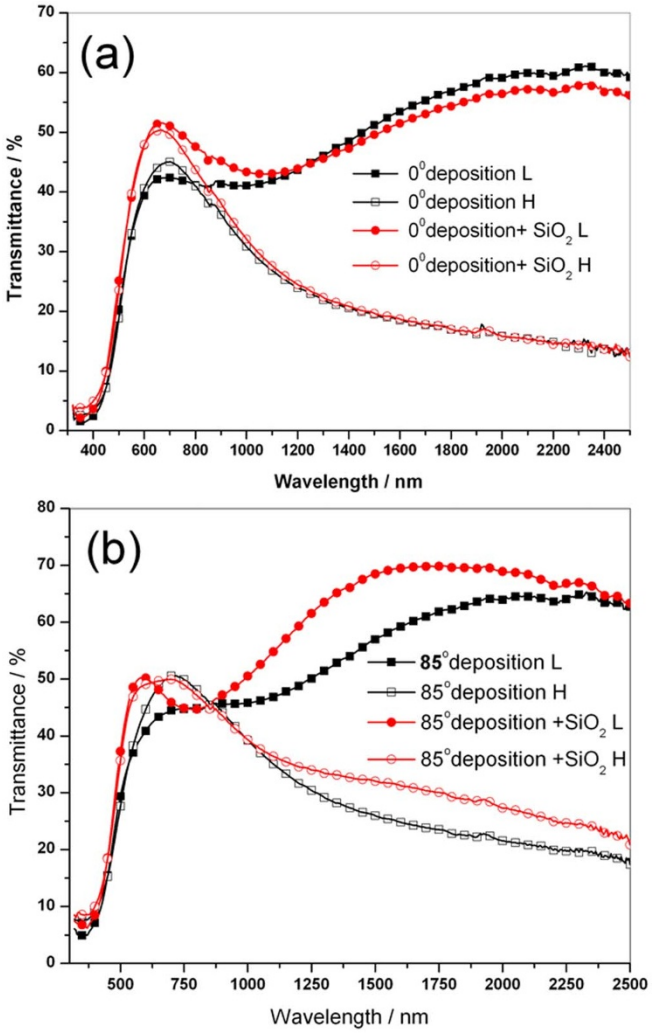

Figure 11 | Transmittance spectra of V_2O_5 STF deposited at 0° and 85° after annealing at 550°C/3 min before and after SiO_2 deposition.

Fig. 13 (e, f). Simultaneously, the polarization effect is more distinct when light is along the direction of columns. For VO_2 deposited at 85° with a layer of SiO_2, the structure of films is changed and the anisotropy is reduced. Thus, the polarization effect and optical anisotropy is not apparent (see **Fig. 13 (i, g, h)**). Due to phase transition of VO_2 films at high and low temperature, the polarization effects need further study in future.

In conclusion, V_2O_5 STF with slanted column structure was prepared by oblique angle thermal evaporation technique. After annealing, V_2O_5 STF can be transformed into VO_2 STF with the melting and aggregation of columnar structure. VO_2 STF with slanted columnar structure can be obtained at 550°C/3 min for V_2O_5 STF deposited at 85°. Due to the porous structure and low refractive index, SiO_2 can be used as effective antireflective layer to improve luminous transmittance and solar modulation ability. After SiO_2 deposition, T_{lum} of VO_2 films deposited at 85° is enhanced 26% (36.9% to 46.6%) and ΔT_{sol} increases 60% (4.5% to 7.2%). Due to the anisotropic column structure, angle selective transmittance is observed for VO_2 (M) STF. The solar modulation ability is further improved for light along the columnar direction especially for VO_2 (M) STF with SiO_2 antireflective layer (7.2% to 8.7%). Moreover, the phase transition temperature of VO_2 STF is greatly depressed into 54.5°C without doping. Considering the oblique incidence of sunlight on windows, VO_2 (M) STF is more suitable as smart window compared with normal homogeneous VO_2 (M) films.

Table IV | T_{lum}, ΔT_{lum}, T_{sol}, ΔT_{sol}, T_{2000}, ΔT_{2000} of V_2O_5 STF deposited at 0° and 85° after annealing at 550°C/3 min before and after SiO_2 deposition

	T_{lum} [%]			T_{sol} [%]			T_{2000} [%]		
	30°C	100°C	ΔT_{lum}	30°C	100°C	ΔT_{sol}	30°C	100°C	ΔT_{2000}
0° VO_2	32.7	33.1	−0.4	35.2	28.6	6.6	59.1	15.9	43.2
0° VO_2 + SiO_2	39.5	39.5	0	39.3	31.7	7.6	56.4	15.8	40.6
85° VO_2	36.9	38.6	−1.7	39.7	35.2	4.5	63.9	21.5	42.4
85° VO_2 + SiO_2	46.6	45.3	1.3	45.1	37.9	7.2	68.9	27.3	41.6

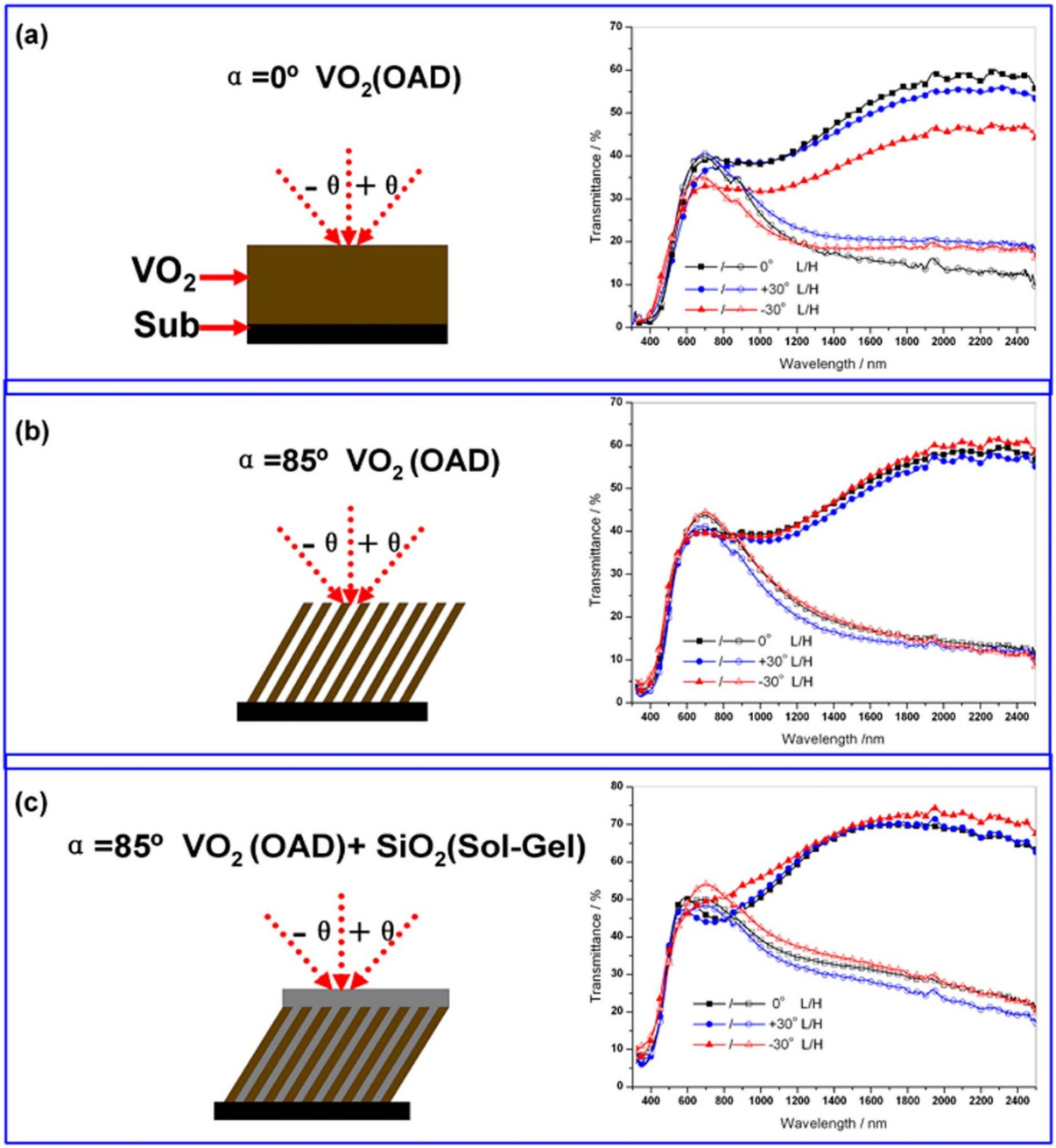

Figure 12 | Transmittance spectra of V_2O_5 STF deposited at 0° and 85° after annealing at 550°C/3 min with testing light incidence angle of 0° and ±30°. (a) VO_2 deposited at 0°; (b) VO_2 deposited at 85°; (c) VO_2 deposited at 85° with a layer of SiO_2.

Table V | T_{lum}, ΔT_{lum}, T_{sol}, ΔT_{sol}, T_{2000}, ΔT_{2000} of V_2O_5 STF deposited at 0° and 85° after annealing at 550°C/3 min with 0° and ±30° incidence testing

		T_{lum} [%]			T_{sol} [%]		
Deposition angle (α)	Testing angle (θ)	30°C	100°C	ΔT_{lum}	30°C	100°C	ΔT_{sol}
0°	0°	24.7	27.5	−2.7	31.3	24.4	6.9
	+30°	22.1	27.3	−5.2	30	25.9	4.1
	−30°	25.1	28	−2.9	27.7	23.3	4.4
85°	0°	33.9	33.6	0.3	34.8	28.4	6.4
	+30°	32.2	32.5	−0.3	33.3	26.3	7.0
	−30°	34.5	34.3	0.2	35.1	29.9	6.1
85° + SiO_2	0°	46.6	45.3	1.3	45.1	37.9	7.2
	+30°	44.6	43	1.3	44.7	35.9	8.7
	−30°	42.8	43.2	−0.4	47.3	39.7	7.6

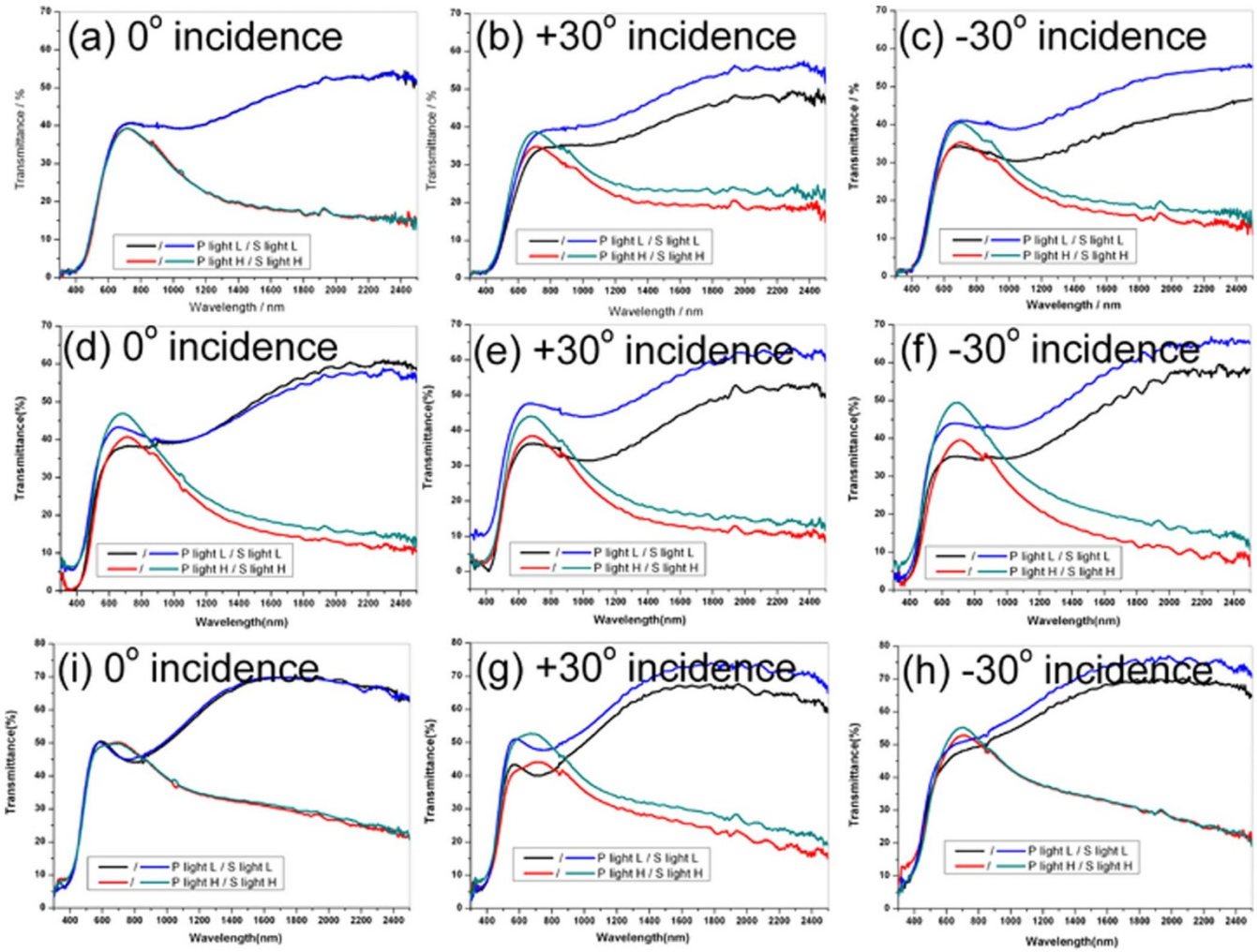

Figure 13 | Polarization transmittance spectra of V_2O_5 STF deposited at 0° and 85° after annealing at 550°C/3 min with testing light incidence angle of 0° and ±30°. (a, b, c) VO_2 deposited at 0°; (d, e, f) VO_2 deposited at 85°; (i, g, h) VO_2 deposited at 85° with a layer of SiO_2.

Methods

Preparation. V_2O_5 sculptured thin films were deposited by thermal evaporation at base pressure of 5×10^{-3} Pa with OAD technique. BK7 glass was ultrasonically cleaned in acetone and ethanol before introducing into the vacuum system. V_2O_5 powder (purity: 99.5%) were evaporated from a tungsten boat located 20 cm from the substrate. The deposition equipment was similar to our previous work[18]. The substrate tilted angle α was measured as the direction of the incident flux with respect to the substrate normal. In our experiment, the deposition angle α was fixed to be 0°, 60°, 80°, 85° without substrate rotation. During deposition, substrate was kept at room temperature. After deposition, V_2O_5 STF was annealed in an infrared lamp heating system (Mila-5000, ULVAC) with heating rate about 50°C/s in hydrogen atmosphere. For antireflective layer deposition, SiO_2 sol was spinning on the surface of VO_2 films at speed of 2000 rpm.

Characterization. The X-ray diffraction (XRD) patterns were obtained on X'Pert Pro MPD diffractometer, using Cu Kα radiation at a scan rate of 0.02° 2θ·S^{-1}. A Hitachi S-4800 scanning electron microscope (SEM) equipped with energy dispersive spectrum (EDS, HORIBA EX-250) was used to acquire SEM images. The thermochromic property was monitored on a PerkinElmer Lambda 750 spectrophotometer equipped with a film heating unit in the wavelength range of 300–2500 nm. Temperature was measured by a temperature sensor in contact with the films and was controlled by a temperature controlling unit. The temperature errors were less than ±2°C. Transmittance spectra before and after phase transition were recorded at low (L) temperature of 30°C and high (H) temperature of 100°C. For the polarization measurement, the polarizer was introduced into the light path. The incident light was two-orthogonal polarization light named as P-light and S-light. The incident light was parallel to the deposition plane.

1. Corr, S. A. *et al.* Controlled reduction of vanadium oxide nanoscrolls: crystal structure, morphology, and electrical properties. *Chem. Mater.* **20**, 6396–6404 (2008).
2. Chen, Z. *et al.* VO_2-based double-layered films for smart windows: optical design, all-solution preparation and improved properties. *Sol. Energ. Mat. Sol. C.* **95**, 2677–2681 (2011).
3. Benkahoul, M. *et al.* Thermochromic VO_2 film deposited on Al with tunable thermal emissivity for space applications. *Sol. Energ. Mat. Sol. C.* **95**, 3504–3510 (2011).
4. Lu, S. W., Hou, L. S. & Gan, F. X. Structure and optical property changes of sol-gel derived VO_2 thin films. *Adv. Mater.* **9**, 244–247 (1997).
5. Mlyuka, N. R., Niklasson, G. A. & Granqvist, C. G. Thermochromic VO_2-based multilayer films with enhanced luminous transmittance and solar modulation. *Phys. Status Solidi A* **206**, 2155–2160 (2009).
6. Mlyuka, N. R., Niklasson, G. A. & Granqvist, C. G. Mg doping of thermochromic VO_2 films enhances the optical transmittance and decreases the metal-insulator transition temperature. *Appl. Phys. Lett.* **95**, 171909–11 (2009).
7. Burkhardt, W. *et al.* Tungsten and fluorine co-doping of VO_2 films. *Thin Solid Films* **402**, 226–230 (2002).
8. Jin, P., Xu, G., Tazawa, M. & Yoshimura, K. Design, formation and characterization of a novel multifunctional window with VO_2 and TiO_2 coatings. *Appl. Phys. A: Mater, Sci. Process* **77**, 455–460 (2003).
9. Xu, G., Jin, P., Tazawa, M. & Yoshimura, K. Optimization of antireflection coating for VO_2-based energy efficient window. *Sol. Energ. Mat. Sol. C.* **83**, 29–32 (2004).
10. Lee, M. H. & Cho, J. S. Better thermochromic glazing of windows with antireflection coating. *Thin Solid Films* **365**, 5–9 (2000).
11. Gao, Y. F. *et al.* Enhanced chemical stability of VO_2 nanoparticles by the formation of SiO_2/VO_2 core/shell structures and the application to transparent and flexible VO_2-based composite foils with excellent thermochromic properties for solar heat control. *Energ. Environ. Sci.* **5**, 6104–61010 (2012).
12. Kang, L. T. *et al.* Nanoporous thermochromic VO_2 films with low optical constants, enhanced luminous transmittance and thermochromic properties. *ACS Appl. Mater. Inter.* **3**, 135–138 (2011).
13. Li, S. Y., Niklasson, G. A. & Granqvist, C. G. Nanothermochromics: calculations for VO_2 nanoparticles in dielectric hosts show much improved luminous

transmittance and solar energy transmittance modulation. *J. Appl. Phys.* **108**, 063525–8 (2010).
14. Robbie, K. *et al*. Ultrahigh vacuum glancing angle deposition system for thin films with controlled three-dimensional nanoscale structure. *Rev. Sci. Instrum.* **75**, 1089–1093 (2004).
15. Popta, A., Hawkeye, M., Sit, J. & Brett, M. J. Gradient-index narrow-bandpass filter fabricated with glancing-angle deposition. *Opt. Lett.* **29**, 2545–2547 (2004).
16. Ertekin, E. & Lakhtakia, A. Sculptured thin film solc for optical sensing of gas concentration. *Eur. Phys. J. Appl. Phys.* **5**, 45–50 (1999).
17. Motohiro, T. & Taga, Y. Thin film retardation plate by oblique deposition. *Appl. Opt.* **28**, 2466–2469 (1989).
18. Xiao, X. D. *et al*. Structure and optical properties of Nb_2O_5 sculptured thin films by glancing angle deposition. *Appl. Surf. Sci.* **255**, 20192–20197 (2008).
19. Kranenburg, V. H. & Lodder, C. Oblique-incidence deposition: a review and new experiment data. *Mater. Sci. Eng. R* **11**, 295–354 (1994).
20. Brian, D. & Michael, B. J. Nanofabrication by glancing angle deposition. *Encyclopedia Nanosci. Nanotechnol.* **6**, 703–726 (2004).
21. Nieuwenhizen, J. M. & Haanstra, H. B. Microfractography of thin films. *Philips Tech. Rev.* **27**, 87–90 (1996).
22. Tait, R. N., Smy, T. & Brett, M. J. Modelling and characterization of columnar growth in evaporated films. *Thin Solid Films* **226**, 196–201 (1993).
23. Hodgkinson, I. & Wu, Q. H. Empirical equations for the principal refractive indices and column angle of obliquely deposited films of tantalum oxide, titanium oxide, and zirconium oxide. *Appl. Opt.* **37**, 2653–2659 (1998).
24. Leroux, Ch., Nihoul, G. & Van Tendeloo, G. From VO_2 (B) to VO_2 (R): theoretical structures of VO_2 polymorphs and in situ electron microscopy. *Phys. Rev. B* **57**, 5111–5121 (1998).
25. Xiao, X. D. *et al*. A facile process to prepare one dimension VO_2 nanostructures with superior metal-semiconductor transition. *CrystEngComm* **15**, 1095–1106 (2013).
26. Xu, G., Jin, P., Tazawa, M. & Yoshimura, K. Thickness dependence of optical properties of VO_2 thin films epitaxially grown on sapphire (0001). *Appl. Surf. Sci.* **244**, 449–452 (2005).
27. Kang, L. T., Gao, Y. F. & Luo, H. J. A novel solution process for the synthesis of VO_2 thin films with excellent thermochromic properties. *ACS Appl. Mater. Inter.* **1**, 2211–2218 (2009).
28. Patridge, C. J., Whittaker, L., Ravel, B. & Banerjee, S. Elucidating the influence of local structure perturbations on the metal-insulator transitions of $V_{1-x}Mo_xO_2$ nanowires: mechanistic insights from an X-ray absorption spectroscopy study. *J. Phys. Chem. C* **116**, 3728–3736 (2012).
29. Jin, P., Nakao, S. & Tanemura, S. Tungsten doping into vanadium dioxide thermochromic films by high-energy ion implantation and thermal annealing. *Thin Solid Films* **324**, 151–158 (1998).
30. Xiao, X. D. *et al*. Anisotropic laser-induced damage threshold and residual stress of TiO_2 sculptured thin films. *J. Nanosci. Nanotechnol.* **13**, 824–828 (2013).
31. Binions, R., Hyett, G., Piccirillo, C. & Parkin, I. P. Doped and un-doped vanadium dioxide thin films prepared by atmospheric pressure chemical vapour deposition from vanadyl acetylacetonate and tungsten hexachloride: the effects of thickness and crystallographic orientation on thermochromic properties. *J. Mater. Chem.* **17**, 4652–4660 (2007).
32. Manning, T. D. & Parkin, I. P. Vanadium oxide thin films on glass and silicon from the atmospheric pressure chemical vapour deposition. *J. Mater. Chem.* **14**, 2554–2559 (2004).

Acknowledgements

This work was supported by the National Natural Science Foundation of China (Nos. 51102235 and 51102096) and Strategic New Industry Core Technology Research Project of Guangdong Province (No. 2011A032304003) and CAS Key Laboratory of Inorganic Coating Materials (No. KLICM-2010-05) and Director Innovation fund of GIEC (No. y007r21001) and State Key Laboratory of Silicate Materials for Architectures (Wuhan University of Technology) (No. SYSJJ2013-04).

Author contributions

X.D.X. proposed and guided the overall project. Y.M.S., G.X., G.P.D., G.Q.C., H.Z., P.Y.L., H.M.Z. and Y.J.Z. performed all the experiments and analyzed the results. All the authors discussed the results. X.D.X. and Y.M.S. wrote the manuscript, with discussion from G.X.

Additional information

Competing financial interests: The authors declare no competing financial interests.

How to cite this article: Sun, Y. *et al*. Anisotropic vanadium dioxide sculptured thin films with superior thermochromic properties. *Sci. Rep.* **3**, 2756; DOI:10.1038/srep02756 (2013).